J|A|C|S ARTICLES

Published on Web 12/30/2008

Electrolyte Tuning of Surfactant Interfacial Behavior for Enhanced Density-Based Separations of Single-Walled Carbon Nanotubes

Sandip Niyogi,† Crystal G. Densmore, and Stephen K. Doorn*

Chemistry Division, Chemical Diagnostics and Engineering (C-CDE) Group, Los Alamos National Laboratory, Los Alamos, New Mexico 87545

Received October 2, 2008; E-mail: skdoorn@lanl.gov

Abstract: We study the interfacial behavior between the straight-chain alkyl surfactant sodium dodecyl sulfate (SDS) and single-walled carbon nanotubes (SWNTs) as a function of added electrolytes, including NaCl. We observe an increase in photoluminescence intensity and narrowing of spectral line widths with electrolyte addition, indicating a change in SDS aggregation number that leads to a pronounced volume change in the nanotube/SDS composite structure. By tuning the interfacial dynamics through NaCl addition and temperature change, we demonstrate that this volume change can be used to yield diameter-dependent separation of metallic and semiconducting SWNTs, without the use of any additional cosurfactant, through density gradient ultracentrifugation. The diameter-dependent fractionation follows the intrinsic relation expected for the density of unfunctionalized nanotubes, indicating a simple amplification of these inherent density differences as the mechanism for salt enhanced separations. Isolation of enriched metallic and semiconducting fractions further illustrates that the surface aggregation characteristics of SDS on metallic SWNTs are different from that on the semiconducting chiralities. These experiments illustrate the governing behavior of surface phenomena and interfacial forces on the diameter-dependent fractionation of SWNTs and point to new routes for enhancing existing separations strategies.

Introduction

The remarkable electronic properties of single-walled carbon nanotubes (SWNTs) hold great promise for revolutionary advances in many applications, including nanoscale electronics, sensors, photonics, and optoelectronics, all of which depend on defined electronic structure and response. However, the realization of this potential has been limited because nanotubes are produced in a broad range of chiralities that include both metallic and semiconducting types with widely varying bandgaps. Separating metallic and semiconducting fractions is fundamentally necessary to exploit nanotube properties for specific applications. Thus, one of the grand challenges of carbon nanotube chemistry has been to separate a nanotube sample into pure fractions of a single chirality or electronic type.

A variety of promising techniques has been developed to separate SWNTs based on their physical and electronic structure.[1,2] One recent development of note has involved differential surfactant functionalization of SWNTs followed by density gradient separations using an ultracentrifuge.[3,4] Density-based separations following other specific covalent and noncovalent functionalization chemistries have also been investigated.[5−7] Density gradient separations (DGS) have found wide use in biochemistry and the pharmaceutical industry. DGS is based on subtle differences in the buoyant densities of mixture components and has drawn attention as a separation method for SWNTs because it is scalable, economical, and compatible with a wide range of nanotube preparation methods that produce different length and diameter distributions. The intrinsic density of SWNTs varies as the inverse of diameter.[3] Therefore, in a liquid column with a designed density gradient along its length, the separation of SWNTs as a function of diameter can be facilitated using centrifugation, with specific nanotube densities fractionating into the matching density of the gradient.[3] Choice of surfactant system in which SWNTs are suspended for DGS processing is critical. For example, simple sodium dodecylsulfate (SDS)−SWNT dispersions do not yield density-based differentiation at 25 °C. Current DGS methods have instead required surface functionalization of SWNTs with complex combinations of SDS, sodium dodecylbenzene−sulfate (SDBS) and bile salts including sodium cholate (SC) to tune the separation.[4,8−10] In other work, ternary cosurfactant combina-

† Current address: Center for Advanced Materials, IACS, Kolkata, India.

(1) Hersam, M. C. *Nat. Nanotechnol.* **2008**, *3*, 387–394.
(2) Krupke, R.; Henrich, F. *Adv. Eng. Mater.* **2005**, *7*, 111–116.
(3) Arnold, M. S.; Stupp, S. I.; Hersam, M. C. *Nano Lett.* **2005**, *5*, 713–718.
(4) Arnold, M. S.; Green, A. A.; Hulvat, J. F.; Stupp, S. I.; Hersam, M. C. *Nat. Nanotechnol.* **2006**, *1*, 60–65.
(5) Chen, Z.; Du, X.; Du, M. H.; Rancken, C. D.; Cheng, H. P.; Rinzler, A. G. *Nano Lett.* **2003**, *3*, 1245–1249.
(6) Maeda, Y.; Kimura, S.; Kanda, M.; Hirashima, Y.; Hasegawa, T.; Wakahara, T.; Lian, Y.; Nakahodo, T.; Tsuchiya, T.; Akasaka, T.; Lu, J.; Zhang, X.; Gao, Z.; Yu, Y.; Nagase, S.; Kazaoui, S.; Minami, N.; Shimizu, T.; Tokumoto, H.; Saito, R. *J. Am. Chem. Soc.* **2005**, *127*, 10287–10290.
(7) Kim, W. J.; Nair, N.; Lee, C. Y.; Strano, M. S. *J. Phys. Chem. C* **2008**, *112*, 7326–7331.
(8) Blackburn, J. L.; Barnes, T. M.; Beard, M. C.; Kim, Y.-H.; Tenet, R. C.; McDonald, T. J.; To, B.; Coutts, T. J.; Heben, M. J. *ACS Nano* **2008**, *2*, 1266–1274.
(9) Green, A. A.; Hersam, M. C. *Nano Lett.* **2008**, *8*, 1417–1422.

10.1021/ja807785e CCC: $40.75

tions of SDS, sodium cholate and deoxycholate were required to isolate pure fractions of metallic SWNTs.[11] In these multicomponent surfactant systems, a structural dependence on the competitive binding of the multiple surfactants to the nanotube allows tuning of specific densities and optimization of the resultant separation.

DGS and other separation techniques rely on a degree of selectivity in surfactant interactions at the nanotube surface. The ultimate success of these techniques is dependent on the dynamic tunability of surfactant surface structures and underscores the importance of gaining a more complete picture of nanotube surface phenomena and interfacial behavior. On graphite surfaces, molecules with long alkyl chains can be adsorbed from solution, forming periodic structures.[12,13] The interaction of the alkyl chain with the hydrophobic surface drives such assembly.[14] The hexagonal carbon lattice forms a curved aromatic surface in carbon nanotubes, but their interaction with ionic surfactant molecules containing long alkyl chains has several similarities with surfactant adsorption on graphite.[15] The alkyl chain adsorbs on the carbon nanotube surface with the ionic headgroup pointing toward water. Analogous to structures found on graphite, TEM analysis shows a structured, nonrandom surface organization.[15] It was observed that SDS molecules organize perpendicular to the nanotube axis with a minimum periodicity of 45 Å. This organization is cooperative, such that the entire nanotube has a unique adsorbed layer structure that follows the SWNT chirality, generating helical striations. Formation of such structures was demonstrated to be highly dependent on headgroup charge, with nonionic surfactants such as Triton X-100 forming a structureless coating over the whole nanotube surface. Such a result implies that changes in effective charge of the headgroup (through electrostatic screening, for example) will have a profound effect on surface structure, adsorbate dynamics, and ultimate density of the nanotube/surfactant hybrid.

In fact, it has been demonstrated on graphite that the presence of electrolytes will reduce the electrostatic repulsion between surfactant head groups, thus leading to an increase in the aggregation number of the surfactant molecules, accompanied by structural changes in the adsorbed patterns.[16] Similar effects are expected on carbon nanotubes. Additionally, above the critical micellar concentration (cmc), the adsorbed structure of SDS on SWNTs was shown to be in dynamic equilibrium between the surface-adsorbed and free molecules.[13,17] Recently, we have demonstrated that this equilibrium can be tuned to yield a diameter-dependent aggregation of nanotubes through successive additions of electrolyte to the nanotube/SDS suspensions.[18] Progressively smaller diameter nanotubes precipitate from suspension as electrolyte concentration is increased. Parallel temperature-dependent behaviors were also observed, in agreement with the expectation that SDS solution solubility will decrease as temperature decreases. In addition to these equilibrium effects, charge screening also plays an important role, with multivalent salts being shown to effect aggregation at much lower concentrations than for monovalent salts like NaCl. The structural dependence found in these effects suggested a role for electrolyte-mediated surfactant manipulation in generating new approaches to the nanotube separations problem.[18] Such electrolyte modulation of the differential surface stabilities of SDBS and flavin mononucleotide has been demonstrated recently as an elegant route to yielding highly enriched samples of the (8,6) chirality.[19] By analogy to the graphite result discussed above, we expect that electrolyte addition will result not only in modulation of nanotube aggregation but also in structural changes of the surfactant assemblies at the nanotube surface, with an accompanying change in overall density of the nanotube/surfactant assembly. Given the ability to tune surface structure and densities in this manner, it may be possible to enhance the DGS approach via incorporation of electrolyte tuning of surfactant equilibria in this process.

In this work we demonstrate that, at electrolyte concentrations below the threshold required to initiate SWNT aggregation, photoluminescence intensity and spectral behavior are consistent with a model that suggests an increase in surfactant packing densities and reorientation at the nanotube surface, as salt concentrations are increased. We exploit the accompanying changes in overall density of the SDS/SWNT composite to enhance the separations capability of DGS. Using 1.25% SDS as the suspension medium, with no incorporation of cosurfactants, we show that addition of appropriate NaCl concentrations can be used in conjunction with ultracentrifugation in a density gradient to fractionate a sample of nanotubes into distinct colored bands. At room temperature, metallic nanotubes are shown to separate from semiconductors, with the metallic species appearing at the lowest gradient densities. Diameter-dependent sorting is also observed within each electronic class, with the largest diameters appearing at the lowest densities. Parallel behaviors are observed at low temperatures (15 °C) in the absence of added salt. The relative ordering of the metallic and semiconductor chiralities in our density gradient separation provides evidence for a higher degree of SDS surface aggregation and larger solvated volume for the SDS−metallic SWNT interaction than for the semiconducting species. The results suggest that electrolyte addition may be a general approach to enhancing DGS for surfactant systems whose adsorption behavior at the nanotube surface may be tuned by electrostatic effects.

Experimental Section

Preparation of SWNT Dispersions. An aqueous suspension of single-walled carbon nanotubes was prepared as follows: 20 mg of HiPco SWNTs (batch no. HPR 107.1) were suspended in 40 mL of D_2O with either 1% or 1.25% (w/v) sodium dodecylsulfate (SDS). The mixture was dispersed with shear mixing at 19 000 rpm (X520 CAT or PowerGen 700D shear mixer) for 1 h followed by tip sonication (Cole Parmer CPX 750) at 35−40 W for 15 min. Alternatively, the mixture was dispersed with bath sonication for 30 min followed by tip sonication at 35−40 W for 30 min. The temperature of the mixture was monitored constantly with a calibrated thermocouple during tip sonication. The temperature was kept below 35 °C by immersing the mixture within an ice−water bath. Immediately after sonication, samples were centrifuged at

(10) Miyata, Y.; Yanagi, K.; Maniwa, Y.; Kataura, H. *J. Phys. Chem. C* **2008**, *112*, 3591–3596.
(11) Yanagi, K.; Miyata, Y.; Kataura, H. *Appl. Phys. Exp.* **2008**, *1*, 034003/1−034003/3.
(12) Groszek, A. J. *Proc. R. Soc. London, A* **1970**, *314*, 473–490.
(13) Rabe, J. P.; Buchholz, S. *Science* **1991**, *253*, 424–427.
(14) Manne, S.; Gaub, H. E. *Science* **1995**, *270*, 1480–1482.
(15) Richard, C.; Balavoine, F.; Schultz, P.; Ebbesen, T. W.; Mioskowski, C. *Science* **2003**, *300*, 775–778.
(16) Wanless, E. J.; Ducker, W. A. *J. Phys. Chem.* **1996**, *100*, 3207–3214.
(17) McDonald, T. J.; Engtrakul, C.; Jones, M.; Rumbles, G.; Heben, M. J. *J. Phys. Chem. B* **2006**, *110*, 25339–25346.
(18) Niyogi, S.; Boukhalfa, S.; Chikkannanavar, S. B.; McDonald, T. J.; Heben, M. J.; Doorn, S. K. *J. Am. Chem. Soc.* **2007**, *129*, 1898–1899.
(19) Ju, S.-Y.; Doll, J.; Sharma, I.; Papadimitrakopoulos, F. *Nat. Nanotechnol.* **2008**, *3*, 356–362.

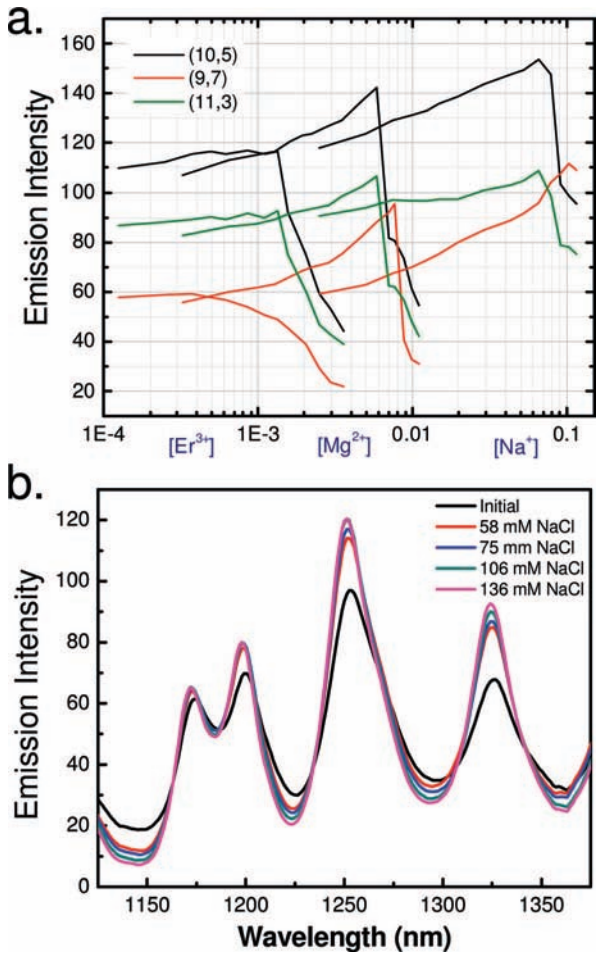

Figure 1. (a) The change in peak photoluminescence intensity at 780 nm excitation of three SWNT chiralities plotted against the molar concentration of $ErCl_3$, $MgCl_2$, or NaCl added to 500 μL of a 1.0% SDS−SWNT dispersion. (b) Photoluminescence spectra at 780 nm excitation for the chiralities of part a. A change in peak width is demonstrated as 58, 75, 106, and 136 mM NaCl is added to 500 μL of a 1.25% SDS−SWNT dispersion.

141 000*g* for 4 h at 25 °C. The upper 75 to 80% of the supernatant was carefully decanted, yielding SDS-dispersed SWNTs.

Salt Titration of SWNT Dispersions (Figure 1). A small volume (1−2 μL) of dilute aqueous solution of NaCl (0.5 to 2.0 M starting concentration), $MgCl_2$ (0.05 M to 0.1M), or $ErCl_3$ (0.005 M to 0.05 M) was added using a microsyringe to 500 μL of SDS−SWNT dispersion in a 5 mm diameter glass tube. After addition of each aliquot, the solution was mixed thoroughly with a vortex mixer. Following each addition, an emission spectrum was collected after the intensity stabilized. The trend was reproduced for multiple batches of SDS−SWNT dispersions. To verify that mere dilution did not impact intensity, small volumes of water (1−2 μL) were added over the same range while monitoring the emission intensity. Addition of water showed very little impact on emission intensity.

Density Gradient Separation (DGS) of SDS−SWNT Dispersions with NaCl. For DGS with added salt, a defined volume of 1 M (aq) NaCl was added to 500 μL of the 1.25% SDS−SWNT dispersion to give the final desired concentration of NaCl. After addition of NaCl, the suspension was stirred for 10−15 min at 800−1000 rpm. The NaCl−SDS−SWNT dispersion was injected carefully above a liquid density gradient column. The density gradient column was formed from manually layering aqueous dilutions of a commercially available 60 (w/v)% aqueous solution of iodixanol (OptiPrep density gradient medium, Aldrich Chemical Co.). Aqueous dilutions of iodixanol were prepared by diluting the 60 (w/v)% OptiPrep stock with 2(w/v)% SDS in H_2O to give 20 (w/v)%, 30 (w/v)% and 40 (w/v)% iodixanol solutions. The density gradient column was formed in Beckman 3 mL capacity thick-wall polyallomer tubes by carefully layering 200 μL 60(w/v)%, 500 μL 40(w/v)%, 500 μL 30(w/v)% and then 300 μL 20(w/v)% at the top. The column was allowed to diffuse for 1 h at room temperature at an angle of approximately 20 degrees from the vertical. After this time, the menisci separating the different density layers were no longer discernible. Following formation of the density gradient column, the NaCl−SDS−SWNT dispersion was carefully injected above the lowest density layer (20 (w/v)% iodixanol) using a syringe. The samples were then centrifuged at 25 °C for 6 h at 250 000*g* (49 000 rpm) using a Beckmann-Coulter SW60Ti swing bucket rotor and a Sorvall WX Ultra 80 centrifuge. Similar experiments were carried out at 22 and 15 °C. The SW60Ti rotor was prechilled for experiments at 15 °C. The centrifugation temperature was verified at 25 °C, 22 °C, and 15 °C by running tubes with mineral oil and measuring the temperature of the mineral oil with a calibrated thermocouple. Following centrifugation, the average SDS concentration across the column was approximately 0.9% (w/v) and gradient linearization was achieved. Pre- and postcentrifugation plots for height vs density can be found in Supporting Information.

Spectroscopic Characterization. After centrifugation, fractions were collected by removing 20 μL − 30 μL portions with a microsyringe or micropipetter. The fractions were diluted with 300 μL of 1% SDS/D_2O for spectroscopy. Absorbance spectra were recorded in a Varian Cary 6000i instrument. Baseline absorbance spectra were collected with a solution of 5% (w/v) H_2O in 1% (w/v) SDS/D_2O for use in spectral subtraction of H_2O contributions to the absorbance of the density gradient samples. Emission spectra (using diode laser exciation at $\lambda_{EX} = 780$ or 658 nm) were recorded using a modified Nicolet NXR-9600 FT-IR spectrometer equipped with a liquid-N_2 cooled germanium detector.[20,21] Spectra were obtained as averages of 64 scans, with a spectral resolution of 4 cm^{-1}. Raman spectra were recorded using Kaiser Optical probehead systems (for laser excitation at 514 and 785 nm) and a SPEX triple monochromator system (for excitation at 633 nm) with CCD detection in all cases. Baseline spectra were collected from a solution of iodixanol, water, and SDS for spectral subtraction of the iodixanol contributions to the Raman data.

Results and Discussion

Interfacial Characteristics of SWNTs Dispersed in SDS Solutions. In aqueous dispersions, SDS bound at the SWNT surface is in equilibrium with free SDS molecules. In pure SDS water solutions above cmc, SDS forms spherical micelles, which transform into cylindrical shapes with the addition of NaCl.[22] On graphite under similar conditions, the interaggregate spacing of adsorbed SDS decreases as the NaCl concentration increases.[16] Thus, the reduction in headgroup electrostatic repulsion due to the addition of NaCl causes an increase in micelle aggregation number and drives more SDS molecules to adsorb on the graphite substrate. Increasing NaCl concentration also leads to an increase in the diameter of the adsorbed phase,[16] and divalent cations induce a similar increase in volume of the adsorbed phase (suggesting a transition from a flat to hemicylindrical curved structure).[23]

When the surface is SWNTs, we observe that the basic interfacial phenomenon remains the same. As shown in Figure

(20) McDonald, T. J.; Jones, M.; Engtrakul, C.; Ellingson, R. J.; Rumbles, G.; Heben, M. J. *Rev. Sci. Instrum.* **2006**, *77*, 053104/1−053104/6.
(21) O'Connell, M. J.; Eibergen, E. E.; Doorn, S. K. *Nat. Mater.* **2005**, *5*, 412–418.
(22) Hayashi, S.; Ikeda, S. *J. Phys. Chem.* **1980**, *84*, 744–751.
(23) Wanless, E. J.; Ducker, W. A. *Langmuir* **1997**, *13*, 1463–1474.

1a, on titrating a SWNT−SDS dispersion with dilute NaCl solution, the emission intensities of all the major chiralities observed at 780 nm excitation initially increase and then abruptly fall below the initial intensity of each chirality. This abrupt loss in intensity corresponds to the previously observed threshold for nanotube aggregation, which in general appears at lower NaCl concentrations as diameter increases.[18] We also note that the position of the intensity maximum with NaCl concentration can vary between SWNT dispersion preparations and includes a dependence on surfactant concentration. Finally, we find that the minor dilution of sample introduced in our titration experiment does not impact the SWNT emission intensity. Adding aliquots of water over the same range shows very little impact on emission intensity.

The behavior of Figure 1a can be understood in terms of tuning of the mean interaction distance between nanotubes. Recent studies of energy transfer between semiconducting nanotubes have shown that exciton energy transfer from small to large diameter nanotubes will suppress emission intensity in the smaller diameters.[24−27] Efficient energy transfer is found to occur only at limited distances (within 2 nm).[25] The results in Figure 1a show that addition of NaCl below the nanotube aggregation threshold serves to modify the surfactant interfacial behavior in a way that increases the mean nanotube interaction distance and consequently minimizes the efficiency of energy transfer. Intertube interactions are also expected to result in a broadening and red-shifting of spectral features.[28,29] In this work, we observe the opposite behavior. Figure 1b shows a decrease in photoluminescence line width (for the chiralities highlighted in Figure 1a) and minor blue-shifting (by 2−3 nm) of the bands as NaCl concentration is increased up to the limit of maximized emission intensity. The line width decrease is evident in the improved resolution and decreased spectral overlap between the peaks shown. These observations are also consistent with our previous work that demonstrated an improved resolution in the nanotube absorption spectrum at NaCl concentrations below the nanotube aggregation threshold.[18] These results lead us to propose a model in which NaCl addition (at concentrations below the aggregation threshold) yields a decrease in nanotube interaction.

Such a decrease in intertube interactions may seem counterintuitive, with an initial expectation that electrolyte screening of surface charges should reduce interaction distance. However, as discussed above for graphite, addition of NaCl to our suspensions is also expected to alter the surfactant structure at the nanotube surface so that SDS packing density is increased (as depicted in our proposed model in Scheme 1). The result is a restructuring that increases the diameter and volume of the nanotube/surfactant aggregate through a transition of the adsorbed SDS from a flat to a curved layer. Additionally, the hydration sphere associated with the Na^+ cation also becomes incorporated into the surfactant structure as additional Na^+ binds to and partially neutralizes the anionic headgroups of SDS.[30] These two mechanisms act in concert to increase the total volume of the adsorbed surfactant layer. The resulting increase in the steric repulsion between individual SDS/SWNT hybrid structures combines with the residual electrostatic repulsion to yield the observed increase in photoluminescence intensity.[30,31] Such steric repulsive forces between surfaces can overcome competing van der Waals attractive forces over 1−3 nm,[31] the same length scale over which efficient energy transfer is expected to occur. We note that the changes in surface structure discussed above should also more efficiently exclude water from the nanotube surface, effectively altering both hydrophobic interactions and dielectric environment. While these effects might also contribute to the spectral changes observed in Figure 1b, the bulk of such water-induced spectral changes are expected to occur below the cmc.[32,33]

Scheme 1. Model for the Fundamental Adsorption Behavior of SDS on SWNTs That Leads to the Observations Reported Here[a]

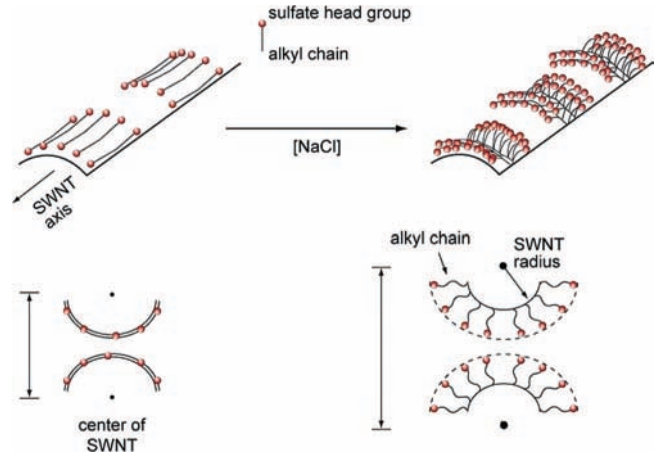

[a] The addition of NaCl leads to increased aggregation of SDS on the nanotube surface, resulting in reorientation from a flat to a curved layer. The transformation of the surfactant layer increases both the total volume of the SDS/SWNT assembly and the average distance between SWNTs, as depicted in the lower cross-sectional view. The result is an amplification of the density differences between SWNTs.

It is instructive to note that the SDS-adsorbed SWNT surface can also be thought of as a polyanion with tightly bound counterions, making the treatment of charge interactions in our model similar in many respects to counterion condensation descriptions of polyion interactions with electrolytes. While in our case the total surfactant headgroup charge is dynamic and tunable by adding electrolyte, once this charge is established by the new equilibrium surfactant structure after salt addition, counterion condensation theory states only a fraction of that charge becomes neutralized through cation binding.[34,35] This is in agreement with our picture of partial headgroup neutralization prior to reaching salt concentrations at which nanotubes aggregate. Within this context, recent atomistic modeling of SDS interactions at graphite surfaces[36] shows that cation condensation

(24) Kato, T.; Hatakeyama, R. *J. Am. Chem. Soc.* **2008**, *130*, 8101–8107.
(25) Qian, H.; Georgi, C.; Anderson, N.; Green, A. A.; Hersam, M. C.; Novotny, L.; Hartschuh, A. *Nano Lett.* **2008**, *8*, 1363–1367.
(26) Tan, P. H.; Rozhin, A. G.; Hasan, T.; Hu, P.; Scardaci, V.; Milne, W. I.; Ferrari, A. C *Phys. Rev. Lett.* **2007**, *99*, 137402/1–137402/4.
(27) Torrens, O. N.; Milkie, D. E.; Zheng, M.; Kikkawa, J. M. *Nano Lett.* **2006**, *6*, 2864.
(28) O'Connell, M. J.; Bachilo, S. M.; Huffman, C. B.; Moore, V. C.; Strano, M. S.; Haroz, E. H.; Rialon, K. L.; Boul, P. J.; Noon, W. H.; Kittrell, C.; Ma, J.; Hauge, R. H.; Weisman, R. B.; Smalley, R. E. *Science* **2002**, *297*, 593.
(29) O'Connell, M. J.; Sivaram, S.; Doorn, S. K. *Phys. Rev. B* **2004**, *69*, 235415.
(30) Sein, A.; Engberts, J. *Langmuir* **1995**, *11*, 455.
(31) Israelachvili, J. N.; Wennerstrom, H. *Langmuir* **1990**, *6*, 873.
(32) Moore, V. C.; Strano, M. S.; Haroz, E. H.; Hauge, R. H.; Smalley, R. E.; Schmidt, J.; Talmon, Y. *Nano Lett.* **2003**, *3*, 1379–1382.
(33) Strano, M. S.; Moore, V. C.; Miller, M. K.; Allen, M. J.; Haroz, E. H.; Kittrell, C.; Hauge, R. H.; Smalley, R. E. *J. Nanosci. Nanotechnol.* **2003**, *3*, 81–86.
(34) Manning, G. S. *J. Chem. Phys.* **1969**, *51*, 924–933.
(35) Manning, G. S. *J. Phys. Chem. B* **2007**, *111*, 8554–8559.
(36) Tummala, N. R.; Striolo, A. *J. Phys. Chem. B* **2008**, *112*, 1987–2000.

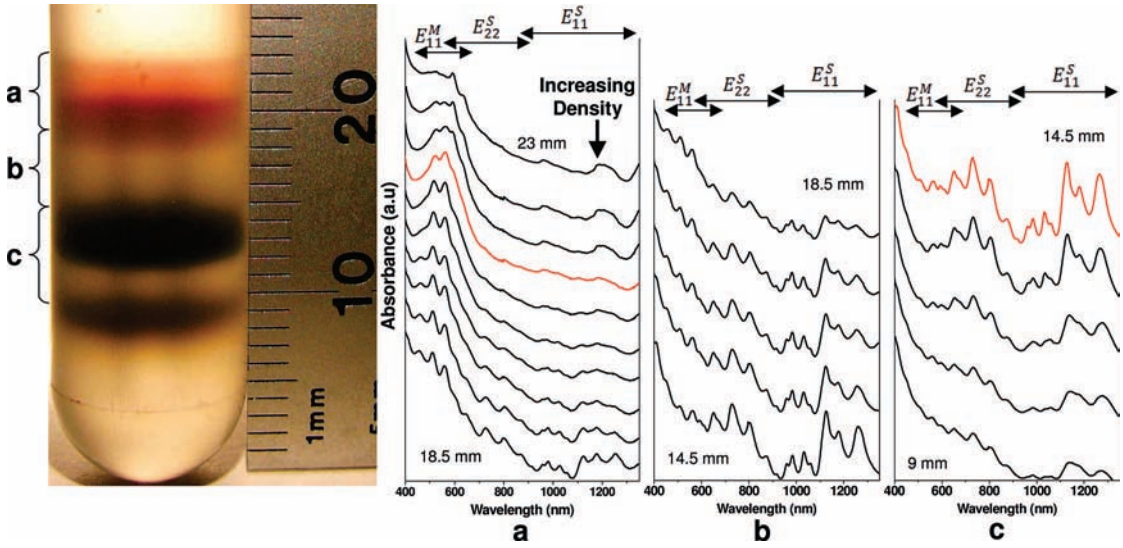

Figure 2. The results of a density gradient separation on a 1.25% SDS−SWNT dispersion with 91 mM NaCl at 25 °C. The photo at left shows fractionation of the initial dispersion into colored bands within the centrifuge tube. Twenty microliter fractions were collected at the same height from four tubes and combined. The combined (80 μL) fractions were diluted with 300 μL of 1% SDS/D_2O for spectroscopy. Absorbance spectra are shown for fractions collected (a) between 18.5−23 mm (from tube bottom), (b) between 14.5−18.5 mm, and (c) 9−14.5 mm. Photoluminescence and Raman spectra are illustrated in Figure 3 for the highlighted (red) fractions shown above.

acts to induce the surfactant volume increases observed experimentally,[16] while also modulating the dielectric environment, as discussed above for water. Furthermore, course grained molecular dynamics simulations of surfactant/SWNT interactions[37] suggest that an increase in surfactant aggregation number leads to a volume increase in the surfactant layer to yield the striated hemicylindrical surfactant structures previously observed at the SWNT surface by Richard et al.[15] Thus, cation condensation and electrolyte-induced increases in SDS aggregation number are seen as the potential mechanistic drivers for the surfactant volume increase we propose in our model. Although there remains some debate over the nature of the initially adsorbed surfactant structure,[15,38] of primary significance in our model is that this initial structure is ultimately transformed to one of greater volume through charge interaction with the added electrolyte.

We find our model also fits the behavior observed with addition of higher valent cations, including Mg^{2+} and Er^{3+}. The photoluminescence behavior upon addition of these species is compared to that of the Na^+ case in Figure 1a. The intensity response with addition of the multivalent cations is less pronounced than with Na^+. A lower maximum intensity is achieved with Mg^{2+} before nanotube bundling occurs, and the response with Er^{3+} remains flat up to the nanotube bundling threshold. This result demonstrates well the competition between the steric repulsive forces and screening of the electrostatic forces that can result in van der Waals attractions dominating the intertube interactions and lead to bundling. As reported previously, bundling sets in at much lower concentrations for the multivalent ions than for Na^+.[18]

The efficiency of incorporation of a cation into the surfactant structure and the resultant screening/neutralization of headgroup charge depends on the cation valency, with the efficiency trend of $M^{3+} > M^{2+} > M^+$. The higher valencies are able to bind multiple surfactant head groups.[39] Additionally, the hydration number for the three cations studied here goes as $Na^+ > Mg^{2+} > Er^{3+}$. Reduction in hydration number is expected to increase binding efficiency at the headgroup as well.[30,40] Based on this solvation effect alone, the volume change of SDS/SWNT hybrid structures with higher valent salts will be smaller than the volume change with Na^+. This volume phenomenon with higher valent cations is due to the reduced number of cations incorporated into the surfactant structure combined with their reduced hydration number. Perhaps more importantly, however, is that the increased screening efficiency found for Mg^{2+} and Er^{3+} allows the system to move to a state in which the van der Waals attractive forces between nanotubes dominate and nanotube bundling results.[18] The bundling occurs before the system enters the surface aggregation regime in which steric repulsion from the volume increase associated with surfactant reorientation can dominate. This condition will result in significantly lower enhancement of the emission signal, as we demonstrate in Figure 1a. The observation of these phenomena fits into a self-consistent model of how the surfactant-nanotube interfacial behavior may be manipulated in the presence of added electrolyte. Because the salt-induced volume changes discussed above can serve to amplify the inherent density differences between SWNTs of different structure, our ability to control cation valency and concentration provides a precise tool to modify the density of the resulting SWNT/SDS composite and differentiate between SWNT structure. We explore this potential in the following sections.

The Differentiation of SWNT Structure. The results of the previous section suggest that salt-induced volume changes within individual hybrid SDS/SWNT structures should be a promising route to enhance separations through density gradient ultracentrifugation. We have found that addition of an appropriate concentration of NaCl to an SDS suspension of SWNTs, prior to loading onto a density gradient, allows the sample to

(37) Wallace, E. J.; Sansom, M. S. P. *Nano Lett.* **2007**, *7*, 1923–1928.
(38) Yurekli, K.; Mitchell, C. A.; Krishnamoorti, R. *J. Am. Chem. Soc.* **2004**, *126*, 9902–9903.
(39) Israelachvili, J. N. *Intermolecular and Surface Forces*, 1st ed.; Academic Press: San Diego, 1985.
(40) Lamont, R. E.; Ducker, W. A. *J. Am. Chem. Soc.* **1998**, *120*, 7602.

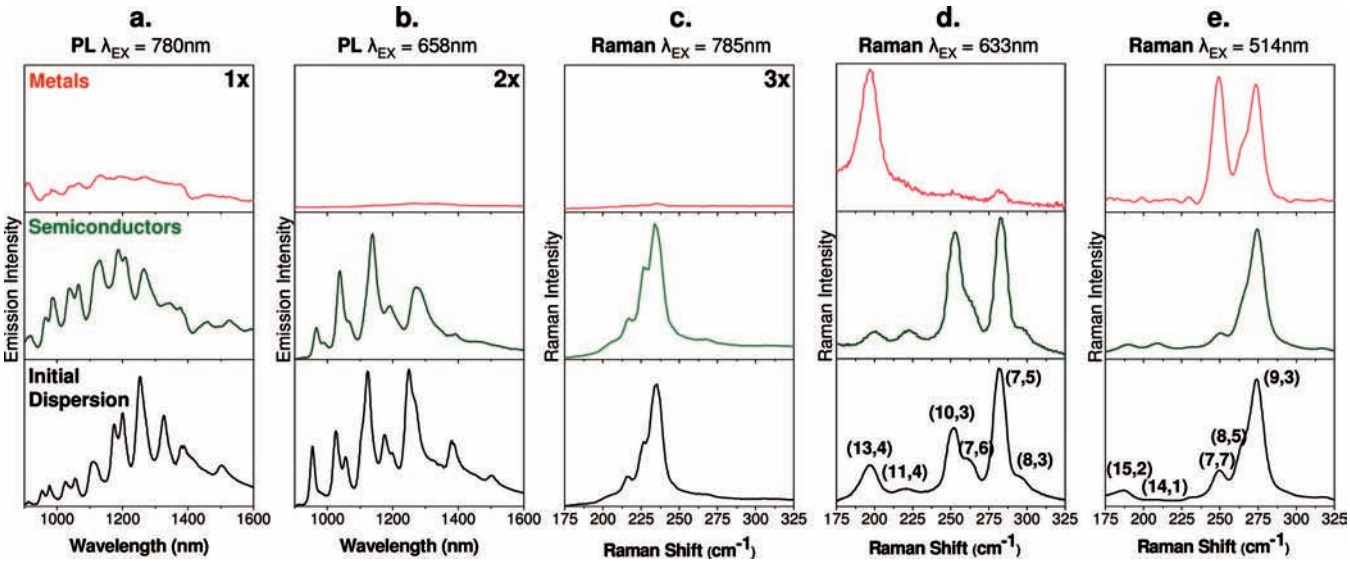

Figure 3. Photoluminescence spectra at (a) 780 nm excitation and (b) 658 nm excitation, and Raman spectra at (c) 785 nm excitation, (d) 633 nm excitation, and (e) 514 nm excitation of metallic and semiconductor fractions and for the initial 1.25% SDS−SWNT dispersion. The metallic and semiconductor spectra are from the fractions corresponding to the red-highlighted absorbance spectra shown in Figure 2a and 2c, respectively. Spectra are normalized to the most intense peak in each with the exception of metals in a, b, and c, which are directly comparable to the corresponding semiconductor fraction with the scale magnification indicated.

fractionate into colored bands upon ultracentrifugation (see Figure 2). The results of Figure 2 were obtained by preparing a 500 μL aliquot of SWNTs in a 1.25% SDS dispersion with 91 mM NaCl. The aliquot is loaded on the top of the density gradient (preparation described in Experimental Section) and centrifuged at 25 °C for 6 h at 250 000g. The same gradient is used for all results described here. Fractionation can be obtained over a range of added NaCl concentrations, but optimal separation occurs at 91 mM, as shown in Figure 2. A plot of photoluminescence intensity vs salt concentration (such as in Figure 1a) at a specific SDS concentration may be used as a qualitative guide for choosing an optimal concentration for fractionation. An analogous plot to Figure 1a for a dispersion in 1.25% SDS (see Supporting Information) shows an intensity peak near 180 mM NaCl for nanotubes centered at a diameter of about 1 nm, such as the (12,1) and (10,5) structures. We find that the lower optimal NaCl concentration we use in Figure 2 allows larger diameters to remain stable under our separation conditions, when they might otherwise bundle at the salt concentration that gives a peak response for smaller diameters.

Figure 2 also shows the absorption spectra of individual fractions collected in 20 μL intervals from the lowest density region (top) to highest density region (bottom). Spectra are sorted into three zones of behavior. Figure 2a shows absorbance spectra of fractions collected between 18.5−23 mm from the bottom of the centrifuge tube (1.10−1.16 g/mL density). Figure 2b shows absorbance spectra of fractions collected between 14.5−18.5 mm from the bottom of the centrifuge tube (1.16−1.18 g/mL). Figure 2c shows absorbance spectra of fractions collected between 9−14.5 mm (1.18−1.26 g/mL). Absorbance spectra at the lowest densities in Figure 2a (corresponding to band colors grading from purple to pink) show features at wavelengths shorter than 700 nm, corresponding to the lowest energy metallic nanotube E_{11}^M transitions (broad peaks occurring at 1000 and 1200 nm are residual H_2O absorbances present from the iodixanol source). Spectra for these lowest density fractions are free of the E_{22}^S and E_{11}^S semiconducting features normally seen in the ∼500 to 900 nm and 900 nm to longer wavelength regions, respectively, in unfractionated nanotube samples. The lowest density fractions in this "metallic" zone are thus highly enriched in metallic nanotubes, with minor semiconducting impurities occurring only in the highest density fractions of Figure 2a. The spectra of all fractions in Figure 2b show a mix of E_{11}^M, E_{22}^S, and E_{11}^S features, indicating a mixture of metallic and semiconducting species, but with a growth in relative amount of semiconductors at the highest densities. Such limitations in resolution may be caused by the density gradient, length distribution of SWNTs, carbonaceous impurities, or top-loading of the unseparated sample onto the gradient (vs isopycnic injection), with all of these factors having been demonstrated to be important in obtaining high resolution separation.[4,11,41] The spectra of Figure 2c are dominated by E_{22}^S and E_{11}^S features, indicating a high degree of semiconductor enrichment, with smaller diameter metallic impurities occurring primarily at the lowest density regions of this "semiconductor" zone (appearing as the very dark green band between 11.5−14.5 mm in the image shown in Figure 2). The broadened spectra in the highest density fractions indicate bundled nanotubes are sorting out at the bottom of the centrifuge tubes.

Fractionation into enriched zones of metallic and semiconductor species is further supported by photoluminescence and Raman spectroscopy of the isolated fractions, as shown in Figure 3. (Spectra shown for metallic and semiconducting fractions in Figure 3 correspond to the respective fractions whose absorbance spectra are highlighted in red in Figures 2a and 2c.) The photoluminescence spectra and the radial breathing mode (RBM) region of the 785 nm excitation Raman spectrum (shown in Figures 3a, 3b, and 3c) are expected to show only features from semiconductor species, which are clearly absent in the spectra from the metallic fraction. Raman spectra taken at 514 and 633 nm excitation wavelengths, however, show a mixed set of features from both metallic and semiconducting chiralities,

(41) Zheng, M.; Jagota, A.; Semke, E. D.; Diner, B. A.; McLean, R. S.; Lustig, S. R.; Richardson, R. E.; Tassi, N. G. *Nat. Mater.* **2003**, *2*, 338.

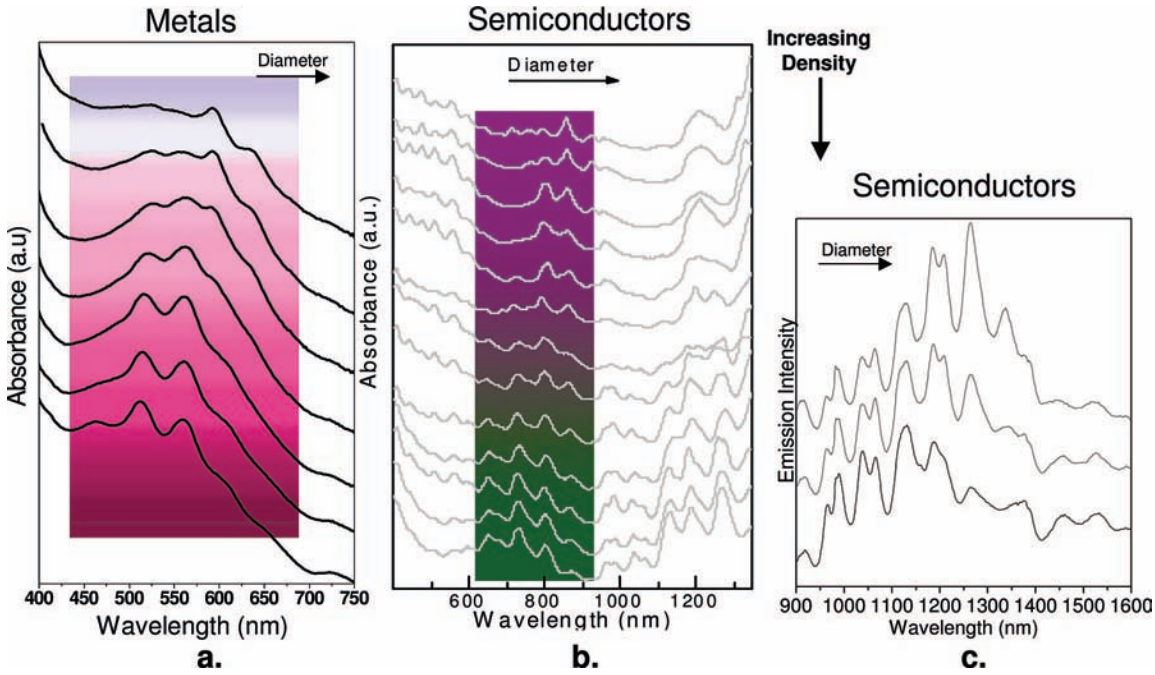

Figure 4. (a) Metallic absorption spectra, (b) semiconductor absorption spectra, and (c) semiconductor photoluminescence ($\lambda_{exc} = 780$ nm) spectra showing nanotube diameter dependence in fractions of increasing density. Fractions in a and c were collected following separation of SDS−SWNT dispersion with 91 mM NaCl at 25 °C at 250 000*g* for 6 h. Part a shows the top seven spectra of Figure 2a but rescaled and highlighted to emphasize the diameter-dependent separation. Semiconductor fractions in part b were collected following separation with 100 mM NaCl at 22 °C at 175 000*g* for 10 h.

which are labeled in the spectra from the unseparated dispersion in Figures 3d and 2e. At 633 nm excitation the metallic fraction is dominated by the RBM of the (13,4) species, with only weak features from the larger diameter semiconductor impurities being present. For the semiconductor fraction, the picture reverses, with the RBM spectrum now being dominated by the resonant semiconductor species. A similar trend is seen for spectra taken with 514 nm excitation. In particular, no semiconductor features are present in the spectrum of the metallic fraction and only begin to appear in the semiconductor fraction. We note that at this excitation wavelength, none of the semiconductor species are expected to show strong, resonantly enhanced RBM intensities.[42] Furthermore, the (14,1) and (15,2) RBM features that do appear are for relatively large diameter nanotubes in the HiPco distribution and are therefore expected to be of low abundance. These effects give rise to the apparently dominant metallic RBM feature in the semiconductor fraction. Nonetheless, it is clear there remains some degree of metallic contamination in even the most highly enriched semiconducting fractions. It is unlikely that the observed changes in RBM spectra (attributed here to changing composition) arise from a change in resonance enhancements that might result from a shift in electronic band position due to salt addition or doping effects.[29] The absorption and emission spectra of Figures 1−3 show no significant shifts in band positions when separated and starting samples are compared.

In addition to sorting by metallicity, diameter fractionation also occurs as a function of density, as shown in Figure 4. An expanded plot of the topmost metallic fractions (Figure 4a) clearly shows a shift in absorption features from low to high energy as one goes to higher densities in the gradient. This shift indicates that the largest diameter metallic nanotubes are found at the lowest densities after fractionation. Similar behavior is found within the semiconductor chiralities, with a shift in both absorption (Figure 4b) and emission (Figure 4c) features to higher energy at higher densities indicating the smallest diameters fractionate at the higher gradient densities. We note that regions of mixed species are composed of the larger diameter semiconductors and smaller diameter metallics. Thus, the fractions most enriched in metals tend to be of larger diameters, while the purest semiconductor fractions tend to be enriched in the smaller diameters. The Raman data in Figure 3 further indicate that smaller diameter nanotubes become concentrated in the highest density fractions. For example, the metallic impurities observed in the higher density semiconducting fraction are from primarily the smaller diameter (9,3) and (8,5) species, while the larger diameter (7,7) chirality is more prominent in the lower density fraction enriched in metallic nanotubes.

Our results show that the largest diameter nanotubes separate into the lowest density fractions, while the smallest appear at higher density, demonstrating consistent separation behavior within each nanotube class (metallic vs semiconductor). Thus, our observations indicate that SDS adsorption does not change the fundamental diameter-dependent density trend expected in bare SWNTs: that their intrinsic density varies as the inverse of diameter.[3] This is a noteworthy contrast to the reported density gradient centrifugation results based on cosurfactant mixtures of SDBS and sodium cholate, in which the diameter-dependent density of the semiconducting SWNTs is reversed in the SWNT−surfactant composites (small diameters separate out at lower densities).[4] Such variations in separations behavior underscore the differences in surfactant interactions at the nanotube surface that we might expect for both pure surfactant systems (SDS vs SDBS) and for the differential interactions expected in cosurfactant systems.

(42) Fantini, C.; Jorio, A.; Souza, M.; Strano, M. S.; Dresselhaus, M. S.; Pimenta, M. A. *Phys. Rev. Lett.* **2004**, *93*, 147406/1–147406/4.

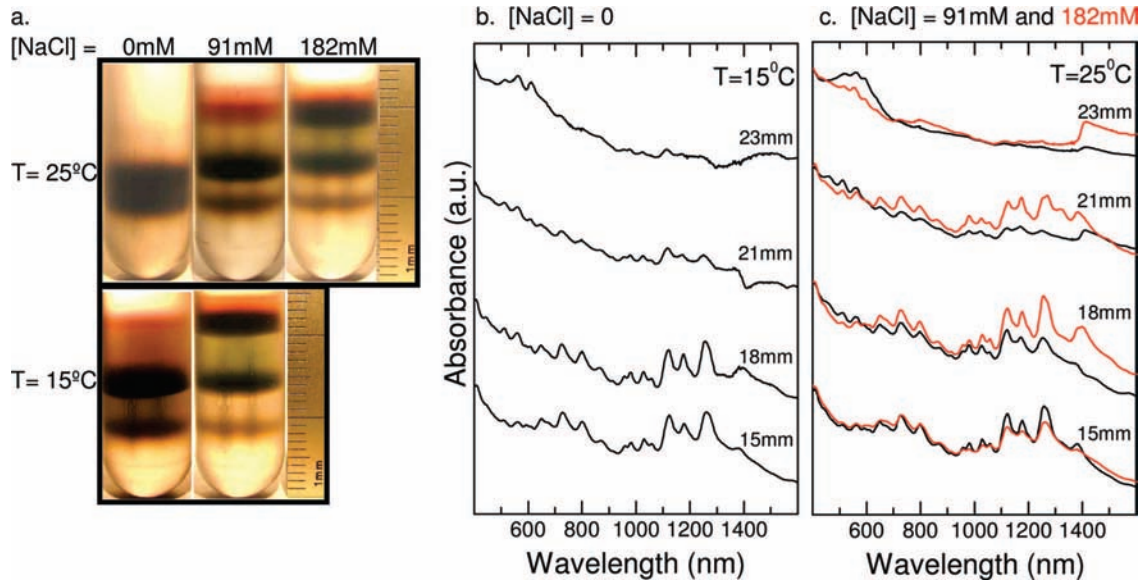

Figure 5. (a) Density gradient separation of 1.25% SDS−SWNT dispersions with 0 mM, 91 mM, and 182 mM NaCl at 25 and 15 °C. Semiconductors are separating into lower density fractions with higher concentrations of NaCl and at lower temperatures. (b) Absorbance spectra of fractions separated at 15 °C (with no added NaCl) and collected at 23, 21, 18, and 15 mm above the tube bottom. (c) Absorbance spectra of fractions separated at 25 °C using 91 mM (black curves) and 182 mM (red curves) NaCl with fractions collected at 23, 21, 18, and 15 mm above the tube bottom.

Our separations results thus provide additional support for the mechanistic picture outlined above and in Scheme 1, in which salt addition increases surfactant packing density, leading to surfactant reorientation at the nanotube surface and an accompanying increase in volume. In this picture, the volume increase accompanying surfactant reorientation must dominate over any increase in density that might result from an increased surfactant packing density. A comparison of Figure 2 to Figure 5a demonstrates this is clearly the case. The metallic and semiconductor fractions have significantly reduced densities (median values of 1.14 g/mL and 1.18 g/mL, respectively) compared to that of the starting nanotube dispersion with no salt added (median value of 1.22 g/mL, see Figure 5a and Supporting Information) after centrifugation. Furthermore, the much larger differential increase in volume available with the greater surface area of a large-diameter nanotube compared to one of small-diameter serves to amplify the already existing inherent density differences between them. An enhancement of their separability within the density gradient results. Such interaction differences are also seen in our ability to differentiate between metallic and semiconducting nanotubes.

Interfacial Characteristics of Metallic and Semiconducting SWNTs Dispersed in SDS Solutions. We find that the ability to discriminate between metallic and semiconducting structures in our salt-enhanced density gradient separations can be understood in terms of a simple extension of our electrostatic model for SDS interfacial behavior. The diameter distribution of metallic nanotubes in the HiPco sample is similar to that of the semiconductors. However, the difference in separation behaviors indicates a fundamental difference in surfactant interactions at these two surfaces. Per our model, as the number of SDS molecules incorporated at the nanotube surface increases, the overall density of the SDS/SWNT composite decreases. The observation that the metallic chiralities separate at the lowest density regions of our gradient column therefore indicates that the metals have an increased packing density of SDS on their surface, relative to the semiconductor surfaces. This indicates a fundamental difference in the adsorption behavior of SDS on metallic versus semiconducting SWNTs and must be accommodated by a difference in surfactant electrostatic interactions between the two species.

Such an effect is in fact expected from the basic principles of electrodynamics. The highly polarizable nature of the metallic nanotube surface permits an approaching point charge (i.e., the anionic headgroup of SDS) to induce a positive image charge at the nanotube surface. This image charge will act to further screen electrostatic interactions between individual SDS molecules,[43] effectively amplifying the screening effects of salt addition. Consistent with our model, this effect ultimately allows an increased SDS packing over what would be expected in the absence of the image charge screening. In contrast, the significantly lower polarizability expected for semiconducting nanotubes (below that of the water medium)[43] may actually act to counter the effective headgroup screening afforded by salt addition and limit the degree to which salt is able to increase SDS packing density at the semiconducting surface, relative to the metallic. Given the opposite direction of such surface-induced electrostatic screening effects, it is therefore not surprising that SDS/metallic nanotube composites are observed here to have such significantly reduced densities compared to semiconductors. Furthermore, we find our model to be consistent with previous theoretical analysis of DNA interactions at the nanotube surface, for which polarizability of the surface also was invoked in order to model the selective separations accessible with DNA wrapping.[43] The recent DGS-based isolation of metallic SWNTs using cosurfactant systems also agrees with this basic phenomenon, although a detailed understanding of the correlation is complicated by the variable behavior expected from the different competing surfactant interactions.[4,8−11] However, the salt-enhanced diameter-dependent separation of metallic SWNTs observed here clearly highlights the effects of the differential polarizability behavior.

(43) Lustig, S. R.; Jagota, A.; Khripin, C.; Zheng, M. *J. Phys. Chem. B* **2005**, *109*, 2559.

Effect of Temperature and NaCl Concentration. The temperature of the solution also has a significant influence on the characteristics of surfactant adsorption on surfaces. A critical temperature is the Krafft point of the surfactant, which controls the dissociation constant and therefore the aggregation number of the surfactant molecules. For example, the Krafft point of 25 mM SDS is 14.36 °C and that of 50 mM SDS is 15.04 °C.[44] Thus, lowering the dispersion temperature can cause changes in the characteristics of the adsorbed molecules similar to the effect of adding salt, including an increase in aggregation number as temperature decreases.[45] We therefore expect to observe parallel temperature-dependent and salt concentration effects in the density gradient behavior; the competing process here is the loss of SDS solubility in D_2O. Of relevance to the cosurfactant systems previously found necessary to isolate pure SWNT fractions, we note that in surfactant mixtures the Krafft point varies as a function of composition.[46]

Previously, we reported that lowering the centrifugation temperature of nanotube suspensions in 1% SDS (and no density gradient) results in the aggregation and coagulation of the largest diameter SWNTs.[18] Furthermore, centrifuging a SWNT−SDS dispersion in a density gradient matrix at 25 °C, without the addition of any salt (Figure 5a), did not result in any separation, as has been reported before.[4] The resulting single black SWNT band is collected at the highest density region of the column. However, at 15 °C in the density gradient, in the absence of any added electrolyte, the SDS dispersion separates into fractions similar to those obtained at 25 °C with added NaCl (Figure 5a). This observation leads us to infer that the SWNT dispersion preparation procedure does not allow differential adsorption of SDS based on SWNT structure to the extent required to induce the volume enhancing surfactant reorientation at the surface. This aspect is related to the association constant of SDS above the critical micelle concentration, which is 0.27 at 25 °C.[47] Abstraction of Na^+ ions from the solution as a route to screening headgroup charge, instead of adding NaCl, could have a similar impact on structure-based differentiation but is not seen to be a significant effect here.

Absorbance spectra of fractions separated at 15 °C, with no added salt, are shown in Figure 5b and show the ability to discriminate between metallic and semiconducting fractions solely by tuning temperature. Cross-contamination of the two types is more evident without the use of salt addition. In part, this is a consequence of a spreading of the semiconductor species over a broader range of densities in the gradient. It is interesting to note that a parallel spreading behavior is observed as one increases salt concentration above our "optimized" value of 91 mM.

In Figure 5a, results from a density gradient separation at 25 °C of the SDS−SWNT dispersion with 182 mM NaCl show that the dark green band (consisting of primarily semiconductors) is resolved at a lower density (approximately 18−21 mm from the tube bottom) than its location upon separation with 91 mM NaCl (approximately 12−15 mm from the tube bottom). Corresponding absorbance spectra for fractions collected at the same height (23, 21, 18, and 15 mm above tube bottom) following separation using 91 and 182 mM NaCl are shown in Figure 5c. For 91 mM NaCl, we achieve good separation of the metallics at the lowest density (approximately 23 mm, 1.10 g/mL). At the same height and density with 182 mM added NaCl, we observe more evidence of small diameter metallics and some large diameter semiconductors. Figure 5c demonstrates that as salt concentration is increased, it is possible to shift diameter distributions into regions of lower density (again consistent with our model for interfacial behavior). This behavior is especially dramatic for semiconductors and is manifested as an increased spreading of diameters over a broader density range.

The simultaneous tuning of interfacial characteristics via both temperature and salt concentration can further accentuate the effects discussed above. As shown in Figure 5a, we find that the effects observed at 182 mM salt concentration and 25 °C can be mimicked at 91 mM with reduced temperature (15 °C). In this case, the semiconducting SWNT chiralities that were separating at higher densities with 91 mM NaCl at 25 °C are now separating into significantly lower density fractions. This combined use of parameters is further illustrated in Figure 4b in which it is seen that even minor temperature changes (to 22 °C in this case) in conjunction with salt use can generate an increased spread in densities that enhance the ability to resolve structural differences within the density gradient. The concerted use of a higher salt concentration and lower temperature may thus be a promising route to increase the resolution between semiconductor diameters but may ultimately be limited to some extent by simultaneous aggregation behavior occurring for the larger diameter nanotubes.[18]

Conclusions

In summary, we have developed a simple qualitative model of SDS interfacial behavior at the nanotube surface in the presence of added electrolyte that parallels similar interactions studied at the graphene interface. Our model is consistent with observations of fluorescence and absorbance behavior that imply a reduction in internanotube interactions upon addition of appropriate levels of metal chloride salts. The increase in SDS/SWNT composite volume that results from modulation of electrostatic interactions between surfactant headgroups and surfactant reorientation in our model has important implications for nanotube separations based on the density gradient ultracentrifugation approach. Thus, we have used the basic principles of this model to demonstrate the use of NaCl in enhancing such separations. As demonstrated here, fractionation of a nanotube sample by metallicity and diameter in a system consisting only of SDS and added electrolyte, without the complicating addition of other cosurfactants, presents significant potential advantages. We find good results may be attained with reduced centrifugation times (~6 h). Of potentially greater significance is that the simplicity of the system allows for easier postseparation processing. There is increasing interest in the use of DGS as a source of metallic and semiconducting material for use in thin film applications.[8−11] Limitations in film performance have been noted as a consequence of incomplete elimination of surfactant from films in postseparation washing steps. A lack of specific surface interaction inherent with SDS, compared to the relative difficulty of surfactant removal with more strongly interacting surfactants, such as cholate, may allow avoidance of this particular complication. The SDS/salt approach to DGS enhancement may therefore be an attractive alternative, particularly after further optimization of the results over a full set of

(44) Vautier-Giongo, C.; Bales, B. L. *J. Phys. Chem. B* **2003**, *107*, 5398.
(45) Benrraou, M.; Bales, B. L.; Zana, R. *J. Phys. Chem. B* **2003**, *107*, 13432–13440.
(46) Tsujii, K.; Saito, N.; Takeuchi, T. *J. Phys. Chem.* **1980**, *84*, 2287–2291.
(47) Bales, B. L. *J. Phys. Chem. B* **2001**, *105*, 6798–6804.

parameters that include centrifugation temperature, salt choice and concentration, and SDS concentration.

Besides the clear applications utility of such separations, we find that the results provide an additional tool for a further understanding of interfacial behavior. In that regard, we find that our separations results further support our model of surfactant reorientation and volume change with added electrolyte. Of particular note is the self-consistency of this picture when surface polarizability effects of nanotube metallicity are introduced. Beyond our qualitative picture, the simple SDS/electrolyte system presented here may be more accessible to theoretical modeling than cosurfactant systems for directing further optimization of the separations. Ultimately, salt enhancement may prove to be of utility in density gradient separations based on cosurfactant systems as well. In that context, gaining a better understanding of surfactant structure and electrolyte effects for single and multiple surfactant systems beyond SDS will be important.

Acknowledgment. We acknowledge useful discussions with J. N. Israelachvili. This work was supported by LANL-LDRD funding.

Supporting Information Available: Additional NaCl titration data for 1.25% (w/v) SDS−SWNT dispersion and pre- and postcentrifugation plots for height vs density of gradients. This material is available free of charge via the Internet at http://pubs.acs.org.

JA807785E